Primary photoexcitations in oligophenylenevinylene thin films probed by femtosecond spectroscopy

G. Cerullo,[1,2,*] G. Lanzani,[1,2] S. De Silvestri,[1,2] H.-J. Egelhaaf,[3] L. Lüer,[3] and D. Oelkrug[3]
[1]*Istituto Nazionale Per la Fisica della Materia, Milano, Italy*
[2]*C.E.Q.S.E. C.N.R., Dipartimento di Fisica, Politecnico di Milano, Piazza L. Da Vinci 32, 20133 Milano, Italy*
[3]*Institute of Physical Chemistry, University of Tübingen, Auf der Morgenstelle 8, 72076 Tübingen, Germany*
(Received 6 January 2000)

The photoexcited state dynamics of vapor-deposited oligophenylenevinylene films, with chain lengths of $n=2$, 3, and 4 vinylene units, is investigated with a 100-fs time resolution. The spectral signatures of three different species A_1, A_2 and A_3 are identified in the photoinduced absorption spectrum. Their assignment is based on kinetics, chain length dependence, and theoretical modeling. A_1 is attributed to the singlet-singlet $S_1 \rightarrow S_2$ transition. The S_1 population displays a strongly intensity dependent decay in the first ps due to bimolecular annihilation. A_2 is assigned to triplet-triplet absorption; the triplet state is populated within the pump pulse duration by a nonconventional mechanism which circumvents the spin-flip constraints. A_3 grows superlinearly with the pump intensity, and shows a distinct formation dynamics. It is assigned to radical ion pairs resulting from singlet coalescence. These results provide insight into the fluorescence quenching mechanisms of organic molecules in the solid state.

I. INTRODUCTION

Organic π-conjugated molecules are very attractive materials for a number of optoelectronic applications, and were recently the object of intense investigations, both theoretical and experimental, aimed at a fundamental understanding of their physical properties. The interest has focused primarily on electroluminescent systems, such as poly(para-phenylene vinylene) and poly(para-phenylene) (PPP).[1] Using these molecules as active media, bright and stable light-emitting diodes were built,[2] and laser action recently demonstrated.[3] In addition, these materials, blended with high electron affinity molecules such as fullerene, show an efficient photoinduced charge transfer,[4] with promising applications in photovoltaic cells. For all the above-mentioned devices, the performance critically depends on the excited-state dynamics. Femtosecond transient spectroscopy is a powerful tool to study these dynamics, and therefore has been extensively applied.[5–11] In spite of the many experimental investigations, however, the question of the number and nature of the primary photoexcitations in electroluminescent polymers still remains open. The generation of emissive intrachain singlet excitons is widely accepted, while the presence of other nonemissive species such as interchain excitons (also known as ''indirect excitons'' or bound polaron pairs), charged species (polarons), and triplet excitons is still under debate. The picture becomes even more obscure at high excitation densities, often reached during device operation: in this case photoexcitation interactions may take place, opening decay channels and/or generating species.

Polymers, in general, show a significant inhomogeneous broadening, resulting from a distribution of conjugation lengths, which smears out the absorption features, both in ground and excited states, making their assignment more difficult. In addition, their dynamics are complicated by spectral relaxation[12] due to the migration of the excitations to lower-energy sites (longer conjugation length chains). These problems can be circumvented by the so-called ''oligomeric approach,'' which consists of investigating oligomeric precursors as model systems with well-defined chain lengths.

In this work, we apply femtosecond pump-probe spectroscopy to the study of excited-state dynamics in thin films of oligo(phenylenevinylene)'s (nPV's) (where *n* is the number of vinylene groups). We examine the three molecules 2PV, 3PV, and 4PV, and find that their photoinduced absorption spectra present common features, which are consistently redshifted, moving from shorter to longer molecules. After photoexcitation, we observe singlet excitons and, with a large yield, the *instantaneous* generation of triplet excitons. At high excitation densities, singlet excitons show a bimolecular decay and concurrently another species is formed, which we identify as polaron pairs resulting from the fusion and subsequent fission of the singlet excitons. Our results provide insight into the singlet exciton deactivation pathways which open up for these materials in the solid phase.

II. EXPERIMENT

Oligo(phenylenevinylene) molecules (see the structure in the inset of Fig. 1) were prepared according to Ref. 13, and amorphous thin solid films ($\approx$100-nm thickness) were deposited onto fused silica substrates.[14] All the experiments were performed in vacuum, to avoid sample photodegradation, and at room temperature. The linear absorption spectra of the nPV films are shown in Fig. 1. In comparison with previous data reported by Woo *et al.*[15] on butyl-substituted oligo-(phenylenevinylene), we note that the spectra of the nPV's show a higher vibronic resolution, due to the better alignment of the unsubstituted molecules.

The femtosecond laser system used for the pump-probe experiments was a mode-locked Ti:sapphire laser with chirped pulse amplification, providing 150-fs pulses at 1.6 eV, with an energy of 700 μJ and a repetition rate of 1 kHz.

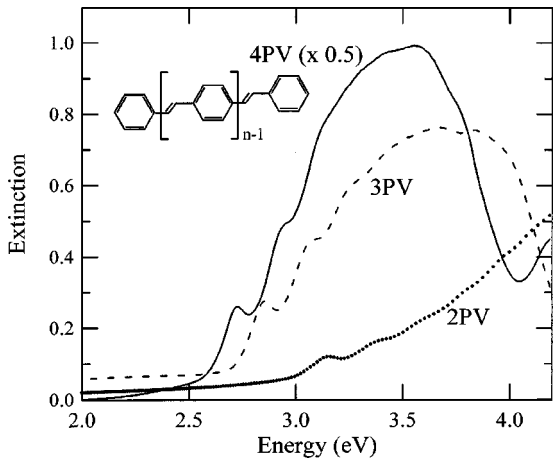

FIG. 1. Extinction spectra of the oligo(phenylenevinylene) films used in the experiments. The inset shows the molecular structure of the nPV's.

Pump pulses at 3.2 eV were obtained by frequency doubling the beam in a 1-mm-thick LiB_3O_5 crystal, while the white-light probe beam was generated by focusing a small fraction (1–2 μJ) of the fundamental beam in a 1-mm-thick sapphire plate.[16] The pump beam was focused to a spot size of 80 μm, and the excitation fluence ranged from 0.1 to 10 mJ/cm^2 per pulse. Mirrors were used to collect the white-light pulse, and to focus it on the sample in order to minimize frequency chirp effects. We performed two different kinds of experiments: (i) For a fixed pump-probe delay, the whole white light pulse was spectrally analyzed after passing through the sample, using a monochromator and a silicon diode array. Transient absorption spectra were obtained by subtracting pump-on and pump-off data over a frequency ranging from 1.3 to 2.9 eV. In these experiments, we measured the differential transmission, defined as $\Delta T/T=(T_{\text{pumpon}}-T_{\text{pumpoff}})/T_{\text{pumpoff}}$; typically we achieved sensitivities of $\Delta T/T\approx 10^{-3}$. (ii) After the sample, the probe beam was passed through interference filters of 10-nm bandwidth, and the differential transmission was measured at a fixed wavelength as a function of pump-probe delay. In this experiment, by chopping the pump beam and using standard lock-in techniques, we could achieve sensitivities down to $\Delta T/T \approx 10^{-5}$.

III. RESULTS

In Fig. 2 we show the $\Delta T/T$ spectra of the 3PV film for different values of the pump-probe delay (τ_D), ranging from 0.5 to 200 ps. The structure of the spectra appears to be quite complex, with several distinct bands displaying markedly different temporal dynamics. Immediately after photoexcitation ($\tau_D=0.5$ ps) we observe three photoinduced absorption (PA) bands, peaking at 1.35 eV (A_1), 1.95 eV (A_2), and 2.7 eV (A_3), respectively. We also observe two increased transmission bands: one at 2.8 eV, which matches the first feature of the ground state absorption spectrum of the molecule, and a weaker one at 2.4 eV. The PA bands display different temporal behaviors: the A_1 and A_3 bands although not with the same dynamics, decay on a 10-ps time scale; while the A_2 band is long lived and is the only absorptive feature surviving at $\tau_D=200$ ps.

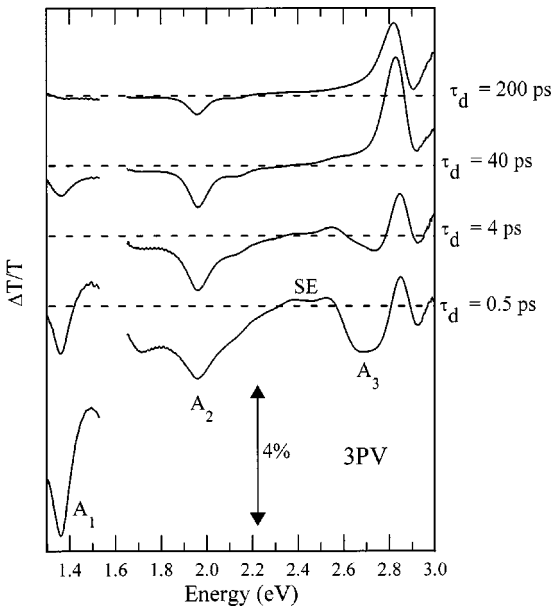

FIG. 2. Differential transmission spectra of a 3PV film excited at 3.2 eV, with a fluence of 3.2 mJ/cm^2 per pulse, for various pump-probe delays τ_D. $A1-A3$ and SE denote the photoinduced absorption bands and stimulated emission, respectively.

Differential transmission spectra for 4PV films as a function of τ_D are shown in Fig. 3: we observe the same features as in 3PV, but redshifted, as expected for a longer chain length. The peak of the A_1 band falls out of our spectral detection window, while the long-lived A_2 band peaks at $\approx$1.8 eV. Finally the third band, A_3, at early times masks the ground-state bleaching, which reappears after its decay. Note that, for comparable excitation levels, the A_2 band appears to be stronger in 4PV with respect to 3PV, which points to a larger yield in the generation of the species responsible for this absorption. A derivative of 4PV, bis-stylbil-2-methoxy-

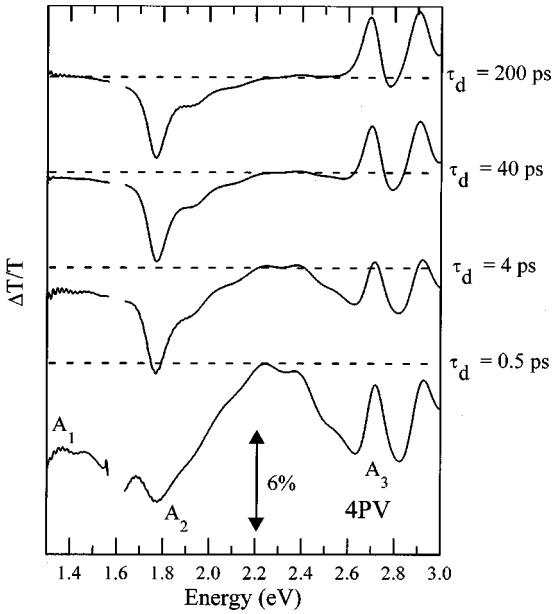

FIG. 3. Differential transmission spectra of a 4PV film excited at 3.2 eV, with a fluence of 3.2 mJ/cm^2 per pulse, for various pump-probe delays.

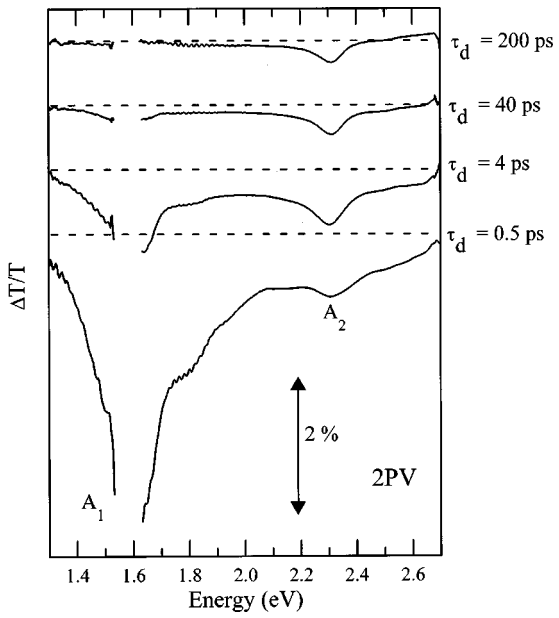

FIG. 4. Differential transmission spectra of a 2PV film excited at 3.2 eV, with a fluence of 5 mJ/cm^2 per pulse, for various pump-probe delays.

5-(2′-ethylhexyloxy)-1, 4-divinylenbenzene (MEH-DSB) was previously studied extensively by femtosecond spectroscopy:[17–19] the differences with our results can be explained by the presence of the side groups in MEH-DSB, which reduce interchain interactions.

Finally, in Fig. 4 we show the differential transmission spectra for a 2PV film: in this case the sample is excited on the red tail of the ground-state absorption, so that bleaching and the A_3 band fall out of our detection range. However, we clearly observe a short-lived A_1 band, peaking at 1.6 eV, and a long-lived A_2 band, peaking at 2.3 eV. Both bands are blueshifted with respect to 3PV and, in this case, the relative strength of the A_2 band is clearly reduced with respect to 3PV.

The three PA bands show markedly different intensity dependences of their kinetics. We will first discuss the case of 3PV. In Fig. 5 we plot as dotted lines the dynamics of the A_1 band at different excitation energies [Figs. (a)–(d)]: we observe that the A_1 band is formed instantaneously upon photoexcitation (also see Fig. 6), and that its decay dynamics is strongly intensity dependent, with faster decays corresponding to higher excitation levels. In Fig. 6 we plot the initial kinetics of the A_2 band compared to that of the A_1 band at the same excitation intensity: also the A_2 band is formed within the pump pulse duration, but it does not display an ultrafast decay. In addition, the dynamics of the A_2 band does not show any significant intensity dependence. For both the A_1 and A_2 bands the differential transmission signal at $\tau_d = 0$ ps grows linearly with the excitation energy. Finally, a striking intensity dependence is displayed by the A_3 band, as shown in Fig. 7. Immediately after excitation a positive ΔT is observed, due to ground-state bleaching, since the probe wavelength (2.7 eV) falls on the tail of the ground-state absorption band. After a few hundred fs an absorptive feature (the A_3 band) is formed, which is superimposed on the positive ΔT. For increasing excitation intensities, the formation time of this band becomes progressively faster and its

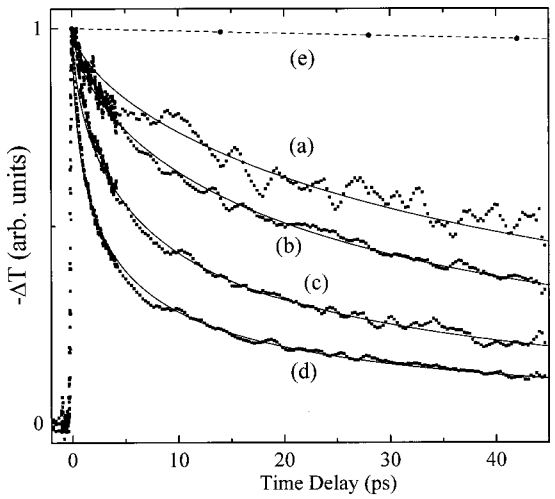

FIG. 5. Points: $\Delta T/T$ vs pump-probe delay in 3PV at 1.38 eV for different pump pulse fluences [(a) 0.1 mJ/cm^2, (b) 0.23 mJ/cm^2, (c) 0.6 mJ/cm^2, and (d) 1.6 mJ/cm^2]. Solid lines: decay curves simulated using the diffusion-controlled annihilation model described in the text [Eqs. (1)–(3)]. (e) displays an experimental fluorescence decay curve (excitation fluence 2×10^{-5} mJ/cm^2).

relative weight increases, so that the overall ΔT signal changes sign turning from photobleaching to photoabsorption. This indicates that the species responsible for the A_3 band is not formed instantaneously, but is a by-product of the primary photoexcitation. After its formation, this species decays with nonexponential dynamics, thus uncovering the bleaching signal, as shown in Fig. 8.

The three PA bands display also the same characteristic intensity dependence in 4PV and 2PV. As an example, in Fig. 9 we plot the decay dynamics in 4PV at the three probe energies 1.46, 1.77, and 2.7 eV, corresponding to the A_1, A_2, and A_3 absorption bands, respectively.

IV. DISCUSSION

In the following paragraphs we propose an assignment of the common features observed in the excited-state transmission spectra of nPV's. The discussion leads to the identifica-

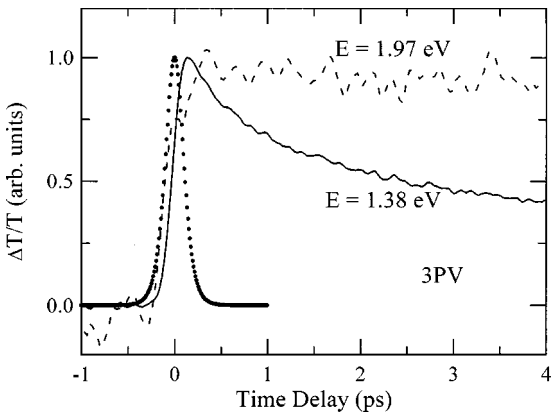

FIG. 6. Normalized differential transmission $\Delta T/T$ vs pump-probe delay in 3PV, probing the A_1 band (solid line, 1.38 eV) and the A_2 band (dashed line, 1.97 eV). Also shown by a dotted line is a typical pump-probe crosscorrelation. The pump pulse fluence is 1.6 mJ/cm^2.

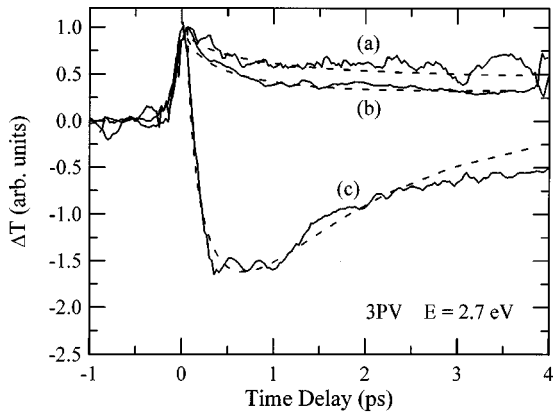

FIG. 7. Solid lines: ΔT vs pump-probe delay in 3PV at 2.7 eV for different excitation fluences [(a) 0.6 mJ/cm^2, (b) 1.6 mJ/cm^2, and (c) 4 mJ/cm^2]. Dashed lines: fits according to the model described in the text.

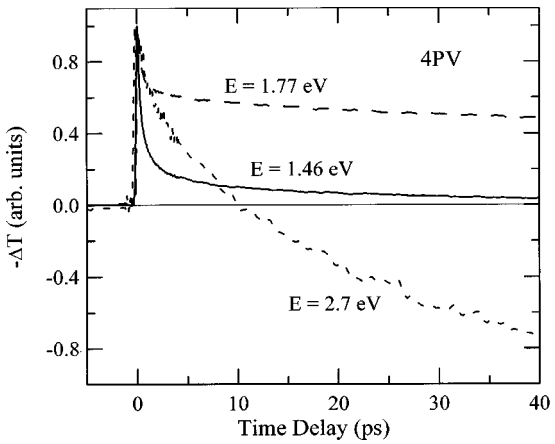

FIG. 9. ΔT vs pump-probe delay in 4PV for different energies probing the three PA features: 1.46 eV (A_1), 1.77 eV (A_2), and 2.7 eV (A_3). The excitation fluence is 3.2 mJ/cm^2.

tion of the elementary species generated by optical excitation and of their dynamics.

A. Assignment of the A_1 absorption band

The $\Delta T/T$ spectra of all nPV samples should display signatures of the lowest singlet excited state, reached after ultrafast thermalization. The increased transmission ($\Delta T>0$) observed in 3PV in the spectral region around 2.4 eV is attributed to stimulated emission (SE) of the $S_1 \rightarrow S_0$ exciton transition, since photoluminescence is observed in this region, with vibronic maxima at 2.55 and 2.39 eV, while no significant ground state absorption is measured (see Fig. 1; any extinction in this region is due to reflection). In Fig. 10 we compare the dynamics of the SE band with that of the A_1 band, under the same photoexcitation conditions: given the almost perfect match, it is straightforward to assign the A_1 band to absorption from S_1 to higher states ($S_1 \rightarrow S_n$ absorption). Based on their dynamics and energetic positions, the A_1 bands of the 2PV and 4PV homologues are assigned to the same $S_1 \rightarrow S_n$ transition as in 3PV. Unfortunately, the A_1 vibronic band is experimentally not completely available in any of the three homologues because of apparative limitations. However, the absorption maxima can be reconstructed from the positions of the first two totally symmetric vibronic sidebands with $\Delta E = 0.16$ eV. After subtraction of an additional $\Delta E = 0.125$ eV, the electronic origins of the A_1 bands are obtained. In Fig. 11 the resulting spectral positions are plotted as diamonds vs the reciprocal chain length $1/m$ (the chain length m is defined as half the number of carbon atoms along the shortest path between the terminal carbon atoms). In Fig. 11 we also plot the energies of the $S_0 \rightarrow S_1$ and $S_0 \rightarrow S_2$ transitions; the latter transition is only very weakly absorbing, but its spectral position can be unambiguously obtained from fluorescence polarization excitation spectra,[20] because the $S_0 \rightarrow S_1$ transition is polarized along the direction of the long molecular axis, and the $S_0 \rightarrow S_2$ transition almost perpendicular to it. Based on semiempirical quantum-chemical calculations on the PPP level, the $S_0 \rightarrow S_1$ transition is assigned to the excitation (1,1*), i.e., the promotion of an electron from molecular orbital (MO) 1 (HOMO, the highest occupied molecular orbital) into MO 1* (LUMO, the lowest unoccupied molecular orbital), while the $S_0 \rightarrow S_2$ transition contains significant contributions from the linear combination (1,2*)-(2,1*).

In the following we will show that the assignment of the A_1 band to the $S_1 \rightarrow S_2$ transition is the most plausible, when its intensity as well as the absolute value and the chain-

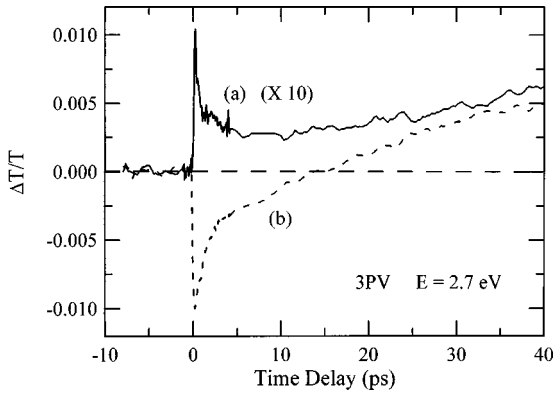

FIG. 8. ΔT vs pump-probe delay in 3PV at 2.7 eV for different excitation energy densities [(a) 0.6 mJ/cm^2 and (b) 6 mJ/cm^2]. (a) is exaggerated by a factor of 10.

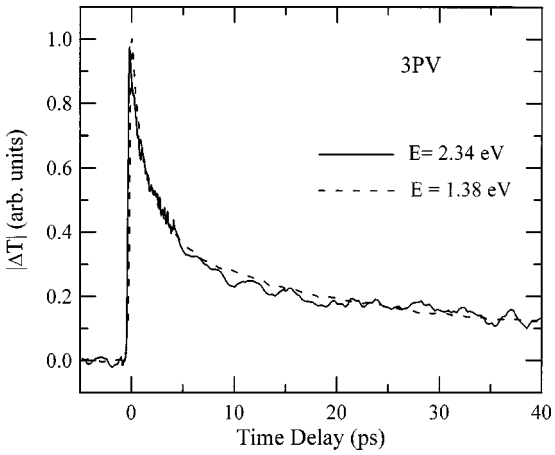

FIG. 10. Modulus of ΔT vs pump-probe delay for 3PV at 2.34 eV (SE, solid line) and at 1.38 eV (A_1, dashed line). The pump pulse fluence is 1.6 mJ/cm^2.

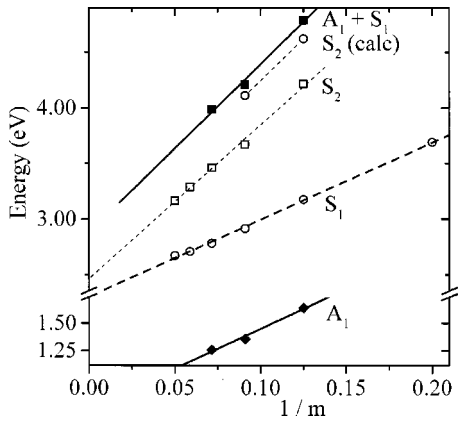

FIG. 11. Energies of electronic transitions in nPV's vs the reciprocal chain length, $1/m$. Symbols represent experimental or calculated data, and lines are linear regressions to the data. A_1 (diamonds) is the photoinduced absorption band A_1 in thin films, S_1 (circles) is the lowest-energetic absorption band of nPV's in solution, S_2 (empty squares)- is the second absorption band of nPV's in solution, and S_2(calc) (circles) is the second absorption band of nPV's in solution as calculated by the PPP method. A_1+S_1 (filled squares)-sum of the transition energies of bands A_1 and S_1. All experimental values refer to band origins, while calculated values refer to band maxima.

length dependence of its spectral position are considered. As illustrated in Fig. 12, the $S_1 \rightarrow S_2$ transition is mainly due to the linear combination (2,1)-(1*,2*), formed by configuration interaction from the degenerate configurations (2,1) and (1*,2*). Both configurations correspond to the promotion of an electron between two energetically adjacent MO's ($\Delta i = 1$). The slope of the chain-length dependence of band A_1 is very similar to that of the $S_0 \rightarrow S_1$ transition, for which $\Delta i = 1$, while it is significantly lower than that of the $S_0 \rightarrow S_2$ transition, for which $\Delta i = 2$.[20,21] As shown in Fig. 11, the sum of the transition energies of the $S_0 \rightarrow S_1$ and the A_1 band actually yields a value close to that of the $S_0 \rightarrow S_2$ transition. Further support to this assignment is provided by the prominent intensity of the A_1 band. As nPV's belong to the point group C_{2h}, only transitions between MO's of different parity are allowed. Due to the alternating parity of the MO's in the frontier orbital region,[20] strong transitions are only possible for $\Delta i = 1$. Other allowed transitions with $\Delta i > 2$ are too weak to account for the strong intensity of the A_1 band, because the overlap of the participating MO's becomes increasingly poorer with growing energetic separation.

B. Singlet exciton dynamics

As already mentioned, the S_1 decay dynamics is nonexponential and strongly intensity dependent, indicating the presence of bimolecular deactivation processes at high excitation levels. This phenomenon, which has been observed in several solid-state organic materials,[22–24] is assigned to the annihilation of singlet excitons, $S_1 + S_1 \rightarrow S_0 + S_n$, where S_n is a higher excited singlet state. In order to model the experimental decay curves, we numerically solve the following rate equation for the concentration of S_1 excitons:

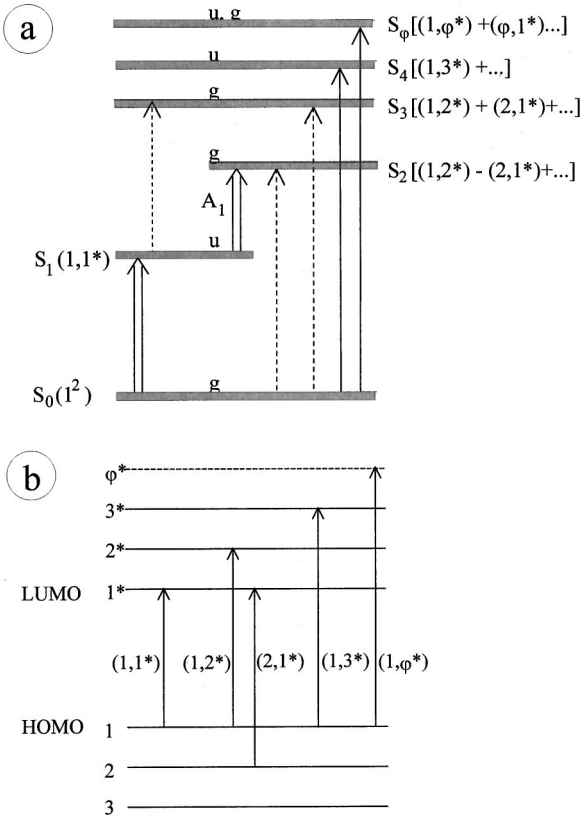

FIG. 12. (a) Electronic states in nPV's with their respective parities u and g. Expressions in brackets give the linear combinations of those configurations which contribute most strongly to a given electronic state. Arrows symbolize electronic transitions. The widths of the arrows correspond to the intensities of the transitions. (b) One-electron configuration of the lowest-energetic singlet transitions. Asterisks denote contributing π^* orbitals.

$$\frac{\partial S_1(z,t)}{\partial t} = \sigma_{01} S_0(z,t) J(z,t) + D_z \frac{\partial^2 S_1}{\partial z^2} - k_m S_1 - \frac{1}{2} k_b(t) S_1^2(z,t). \quad (1)$$

In Eq. (1) the concentration profile of S_1 states along the surface normal is taken into account by dividing the film into thin layers with different distances z from the film surface, and integrating Eq. (1) for each layer separately. The first term on the right-hand side of Eq. (1) describes the generation of S_1 states by $S_0 \rightarrow S_1$ absorption with an extinction coefficient of σ_{01}. The depth profile of the photon fluence, $J(z,t)$, is calculated from Lambert-Beer's law,

$$\frac{\partial J(z,t)}{\partial z} = -\sum_i \sigma_i X_i J(z,t), \quad (2)$$

where X_i and σ_i represent the concentrations and extinction coefficients, respectively, of all absorbing species present in the film. The second term in Eq. (1) takes into account the diffusion of S_1 excitons between different layers. The diffusion coefficient is assumed to be isotropic, i.e., $D_z = D$. The third term describes monomolecular deactivation of S_1 excitons by radiative and nonradiative decay. The mean rate constant for this first-order process, $k_m = 8 \times 10^{+8}\,\mathrm{s}^{-1}$, is ex-

tracted from fluorescence decay curves, obtained at very low excitation levels (an example of which is shown in Fig. 5 as a dashed line). The last term in Eq. (1) represents the bimolecular deactivation process $S_1+S_1\rightarrow S_0+S_n$. Several mechanisms of singlet-singlet annihilation have been proposed in the literature in order to quantitatively describe the kinetics of bimolecular S_1 decays. In organic crystals, diffusion controlled singlet-singlet annihilation is often encountered.[25] In crystalline C_{60} (Ref. 22) and in PPV (Ref. 24) long-range energy transfer (Förster transfer) was suggested to be the dominating mechanism. Depending on the actual mechanism, the bimolecular deactivation constant $k_b(t)$ takes on different forms.

For diffusion-controlled annihilation processes the bimolecular rate constant k_b is given by

$$k_b^{\mathrm{diff}}(t)=8\pi D r_{AB}[1+r_{AB}(2\pi Dt)^{-1/2}], \tag{3}$$

where D is the diffusion coefficient of an S_1 exciton and r_{AB} is a fixed reaction radius, at which annihilation occurs with unity efficiency. The calculated curves, fitted to the experimental decay curves according to Eqs. (1)–(3), are shown in Fig. 5 as solid lines. From these fits, diffusion coefficients in the range of $D=5.10^{-4}-8.10^{-4}\,\mathrm{cm^2\,s^{-1}}$, and reaction radii of $r_{AB}=1.4-1.5\,\mathrm{nm}$ are obtained.

If Förster transfer is the dominant mechanism of annihilation, k_b becomes

$$k_b^F(t)=\frac{2\pi^{3/2}}{3}R_0^3\tau_F^{-1/2}t^{-1/2}, \tag{4}$$

where R_0 represents the critical distance for long-range energy transfer. The best fits using this decay law show significantly steeper initial slopes than the experimental curves, and yield Förster radii between $R_0=4.5\,\mathrm{nm}$ and $R_0=5\,\mathrm{nm}$. These are larger than the Förster radii of $R_0\approx 2\,\mathrm{nm}$, which are estimated from the overlap of the fluorescence spectrum with the A_1 absorption band. Dogariu, Vacar, and Heeger[24] found similarly large Förster radii from the kinetics analysis of S_1 decay curves in PPV, which they explained by invoking spatially delocalized excitonic wave functions.

Diffusion-enhanced Förster transfer combines long-range energy transfer with delocalization of the excitations by diffusion. In this case, the rate constant is given by[26]

$$k_b^{\mathrm{deF}}(t)=4\pi 0.676 D^{3/4}R_0^{3/2}\tau_F^{-1/4}+k_b^F(t). \tag{5}$$

Fit curves (not shown in Fig. 5) and diffusion coefficients resulting from this model are almost identical to those obtained from Eq. (3) for purely diffusion-controlled annihilation. The calculated Förster distances in this case are in the range of $R_0=3.5-4\,\mathrm{nm}$, still not matching the spectroscopical figure.

Which mechanism of exciton-exciton annihilation is operative in nPV's cannot be decided conclusively, mainly due to the small dynamic range of the A_1 decay curves. Moreover, several unknown variables may affect the S_1 decay kinetics. For instance it is known from fluorescence depolarization experiments that there is a considerable degree of short-range order in the films,[27] which may render the rate constants of energy transfer strongly anisotropic.

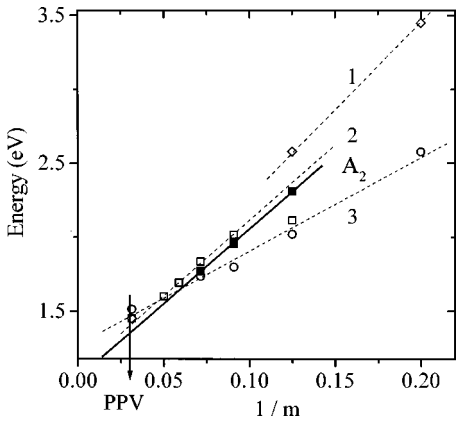

FIG. 13. Energies of electronic transitions in nPV's and PPV vs the reciprocal chain length $1/m$. Symbols represent experimental data, and lines are linear regressions. A_2 (full squares) is the photoinduced absorption band A_2 in thin films. (1) (diamonds) TTA in solution (data for 1PV taken from Ref. 28 and for 2PV from Ref. 29). (2) (open squares) TTA of nPV microcrystals in KBr (from Ref. 15). (3) (circles) $D_0\rightarrow D_2$ absorption bands of nPV radical ions adsorbed onto silica gel (data taken from Refs. 29 and 32). The chain length of the PPV species has been estimated as $n=10$. The PPV data have been taken from Refs. 33 (polaron, TTA), 30 and 31 (TTA), and 34 (polaron).

Despite these uncertainties, there is ample evidence, from the kinetic analysis described above, that exciton diffusion plays an important role in the S_1-S_1 annihilation in nPV's. The annihilation models involving diffusion render satisfactory fits to the experimental curves, with diffusion constants, which are in the range typically encountered in organic solids. In contrast, the kinetic analysis based on pure Förster transfer yields only moderate fits, with Förster radii greatly exceeding those calculated from spectral overlap.

C. Triplet excitons generation in nPV's

The long-lived photoinduced absorption band A_2 is tentatively assigned to triplet-triplet transitions $T_1\rightarrow T_n$. This assignment is based on a comparison of the spectral positions of the A_2 band with those of photoinduced absorption features obtained on nPV molecules and microcrystals as well as on PPV films. Figure 13 shows (full squares) the spectral position of the A_2 band origins, together with those of triplet-triplet absorption (TTA) bands, measured in nPV (Refs. 28, 29, and 15) and PPV (Refs. 30 and 31) species by other techniques. Isolated charged doublets (i.e., radical ions) are excluded by comparison with the absorption data of photogenerated $\mathrm{nPV^+}$ radical cations on silica surfaces [obtained by two-photon absorption after high intensity irradiation at 3.5 eV (Ref. 32)] and of polarons in PPV.[33,34] These samples show two absorption bands, one of them in the near infrared and another one in the visible region of the spectrum, which are due to $D_0\rightarrow D_1$ and $D_0\rightarrow D_2$ transitions, respectively. The energetic positions of the $D_0\rightarrow D_2$ transitions are presented in Fig. 13 as circles. As $D_0\rightarrow D_2$ and $T_1\rightarrow T_n$ transitions are relatively close in energy, the chain-length dependence of the transition energies is a more reliable criterion for assignment than their absolute spectral positions. The slope of the chain-length dependence of the TTA band is

significantly steeper than that of the radical ion absorption, presumably because $\Delta i > 1$ for the $T_1 \rightarrow T_n$ transition, while the $D_0 \rightarrow D_2$ transition corresponds to the excitation $1 \rightarrow 1^*$, for which $\Delta i = 1$. For small nPV's, the $D_0 \rightarrow D_2$ transition lies below the TTA, whereas for chain lengths of approximately $n > 7$, the energetic ordering is reversed. The chain-length dependence of band A_2 is very similar to that of the TTA band, but significantly greater than that of the $D_0 \rightarrow D_2$ transition. Moreover, in the case of 3PV and 4PV, the A_2 band origins observed in our experiments are practically in the same spectral positions as the TTA signals obtained by Woo *et al.*[15] on nPV microcrystals in KBr.

Both the differential transmission spectra (Figs. 2–4) and the time traces (Fig. 6) show that the triplet feature is already present at zero time delay, thus calling for an efficient ultrafast triplet formation mechanism. Several such mechanisms have been proposed in the literature: singlet exciton fission,[35] singlet fusion with subsequent fission into correlated polaron pairs,[35] and singlet exciton breaking into polarons with a subsequent nongeminate bimolecular recombination of polarons into triplet and singlet excitons following spin statistics.[36] We can exclude singlet fusion, because in this case the triplet yield would depend quadratically on the excitation energy, while we observe linear generation. The lack of a clear nPV^+ absorption argues against the polaron recombination mechanism. We thus favor singlet fission as the dominating mechanism of triplet formation. This hypothesis is supported by the observation that the intensity of band A_2, i.e., the triplet yield, increases strongly with the chain length of the nPV's, i.e., with decreasing $S_0 - S_1$ separation. This dependence of triplet yield on the amount of excess energy after excitation indicates that fission takes place directly from vibrationally excited levels of the nonrelaxed S_1 state.

D. Charge photogeneration in nPV's

The nonlinear formation of the species responsible for the A_3 band appears to be strictly related to the bimolecular decay of the singlet exciton. We propose to assign the A_3 band to polaron pairs resulting from the mutual Coulomb attraction of two oppositely charged polarons generated by the reaction

$$S_1 + S_1 \rightarrow S_1^* \rightarrow P^+/P^-, \tag{6}$$

where S_1^* is a singlet excited state with a high enough energy to undergo autoionization into P^+/P^- pairs. Due to the strong correlation the two charged species are not free or isolated, but bound into an overall neutral charge-transfer state. Polaron pairs display a high-energy absorption band which is blueshifted by 0.6–0.7 eV with respect to the corresponding high-energy polaron absorption band.[37] The absorption spectra of singly charged nPV^+ molecules (see the circles in Fig. 13) show high-energy bands peaking at 2.05 and 1.85 eV for $3PV^+$ and $4PV^+$ respectively,[32] so that the expected polaron pair absorption in these materials matches the A_3 band fairly well. The extraction of the polaron pair dynamics is complicated by the overlap of polaron pair absorption and ground-state bleaching. The differential transmission signal A_3 can be written as

$$\frac{\Delta T}{T} \propto \sigma_G(S_1 + T_1 + P) - \sigma_P P, \tag{7}$$

where $\sigma_G(\sigma_P)$ are the ground-state (polaron pair) absorption cross sections, and S_1, T_1, and P are the singlet state, triplet state, and polaron pair populations, respectively. Assuming that the polaron pairs are formed through the bimolecular interaction of singlet excitons, we can write the following rate equation for them:

$$\frac{dP}{dt} = k_b(t) S_1^2 - \frac{P}{\tau_{PP}}, \tag{8}$$

where, for simplicity, we have assumed an exponential decay rate of P, being mainly interested in the formation dynamics of the polaron pairs. The results of the fits, using the parameters derived from the A_1 kinetics for $k_b(t)$, are shown in Fig. 7 as dashed lines. Using the simple rate equation (8) and assuming no decay of the triplet population on the time scale of the experiment, we can reproduce the formation of the A_3 band fairly well, thus supporting our assignment.

V. CONCLUSIONS

In this work we reported on femtosecond pump-probe experiments on nPV thin films with three different chain lengths: the chain length dependence, a comparison with previous spectroscopical data, and theoretical modeling are used to identify the primary excitations. We rationalize the results proposing that photoexcitation generates triplet states and, at high excitation density, polaron pairs together with the expected singlet states. The latter, being the only ones directly coupled to the optical transition, are populated instantaneously by the pump pulses. Triplet states would be formed during a relaxation of the singlet population within 100 fs following optical excitation. This observation strongly supports the proposal that in conjugated systems there are ultrafast relaxation paths alternative to spin-orbit coupling spin-flip paths, which change the state multiplicity. We conjecture that the mechanism active in nPV's is fission of the vibrationally hot S_1 state into triplet pairs. This process, if confirmed, is a relaxation path that opens up in the condensed phase and competes with radiative decay, thus reducing the emission quantum efficiency. At a high excitation density, a condition relevant to the development of organic lasers based on conjugated materials, singlet-singlet interactions, become important. We characterize their dynamics, and propose that singlet fusion generates polaron pairs. These states are rather short lived, but it is plausible that a small fraction of them survives at longer time and eventually separates into charged species. The results can be extended to longer chains, indicating that singlet fusion is an intrinsic channel for the photogeneration of charges in PPV.

All the results here reported provide insight into the photophysics of π-conjugated chains. In particular we elucidate which mechanisms contribute, in the solid state, to reduce the singlet exciton population and thus the luminescence quantum efficiency. The definitive assignment of the observed photoexcitations may be achieved by carrying out more focused experiments, such as electric-field-assisted pump-probe spectroscopy.

*Email address: giulio.cerullo@polimi.it

[1] R. W. Friend, R. W. Gymer, A. B. Holmes, J. H. Burroughes, R. N. Marks, C. Taliani, D. D. C. Bradley, D. A. Dos Santos, J. L. Bredas, and M. Loegdlum, Nature (London) **397**, 121 (1999).
[2] J. H. Burroughes, D. D. C. Bradley, A. R. Brown, R. N. Marks, K. Mackay, R. H. Friend, P. L. Burn, A. Kraft, and A. B. Holmes, Nature (London) **347**, 539 (1990).
[3] N. Tessler, G. J. Denton, and R. H. Friend, Nature (London) **382**, 695 (1996).
[4] N. S. Saricifci, L. Smilowitz, A. J. Heeger, and F. Wudl, Science **258**, 1474 (1992).
[5] M. Yan, L. J. Rothberg, F. Papadimitrakopoulos, M. E. Galvin, and T. M. Miller, Phys. Rev. Lett. **72**, 1104 (1994).
[6] J. M. Leng, S. Jeglinski, X. Wei, R. E. Benner, Z. V. Vardeny, F. Guo, and S. Mazumdar, Phys. Rev. Lett. **72**, 156 (1994).
[7] M. Yan, L. J. Rothberg, E. W. Kwock, and T. M. Miller, Phys. Rev. Lett. **75**, 1992 (1995).
[8] J. W. Blatchford, S. W. Jessen, L. B. Lin, J. J. Lih, T. L. Gustafson, A. J. Epstein, D. K. Fu, M. J. Marsella, T. M. Swager, A. G. MacDiarmid, S. Yamaguchi, and H. Hamaguchi, Phys. Rev. Lett. **76**, 1513 (1996).
[9] N. T. Harrison, G. R. Hayes, R. T. Phillips, and R. H. Friend, Phys. Rev. Lett. **77**, 1881 (1996).
[10] G. Denton, N. Tessler, N. T. Harrison, and R. H. Friend, Phys. Rev. Lett. **78**, 733 (1997).
[11] S. V. Frolov, M. Liess, P. A. Lane, W. Gellermann, Z. V. Vardeny, M. Ozaki, and K. Yoshino, Phys. Rev. Lett. **78**, 4285 (1997).
[12] R. Kersting, U. Lemmer, R. F. Mahrt, K. Leo, H. Kurz, H. Bässler, and E. O. Göbel, Phys. Rev. Lett. **70**, 3820 (1993).
[13] R. Schenk, H. Gregorius, K. Meerholz, J. Heinze, and K. Müllen, J. Am. Chem. Soc. **113**, 2634 (1991).
[14] D. Oelkrug, A. Tompert, J. Gierschner, H.-J. Egelhaaf, M. Hanack, M. Hohloch, and E. Steinhuber, J. Phys. Chem. B **102**, 1902 (1998).
[15] H. S. Woo, O. Lhost, S. C. Graham, D. D. C. Bradley, R. H. Friend, C. Quattrocchi, J. L. Bredas, R. Schenk, and K. Müllen, Synth. Met. **59**, 29 (1993).
[16] G. Cerullo, S. Stagira, M. Nisoli, S. De Silvestri, G. Lanzani, G. Kranzelbinder, W. Graupner, and G. Leising, Phys. Rev. B **57**, 12 806 (1998).
[17] V. I. Klimov, D. W. McBranch, N. N. Barashkov, and J. P. Ferraris, Chem. Phys. Lett. **277**, 109 (1997).
[18] E. S. Maniloff, V. I. Klimov, and D. W. McBranch, Phys. Rev. B **56**, 1876 (1997).
[19] V. I. Klimov, D. W. McBranch, N. N. Barashkov, and J. P. Ferraris, Phys. Rev. B **58**, 7654 (1998).
[20] H.-J. Egelhaaf, L. Lüer, A. Tompert, P. Bäuerle, K. Müllen, and D. Oelkrug, Synth. Met. (to be published).
[21] D. Oeter, H.-J. Egelhaaf, Ch. Ziegler, D. Oelkrug, and W. Göpel, J. Chem. Phys. **101**, 6344 (1994).
[22] S. L. Dexheimer, W. A. Vareka, D. Mittleman, A. Zettl, and C. V. Shank, Chem. Phys. Lett. **235**, 552 (1995).
[23] G. Lanzani, M. Nisoli, S. De Silvestri, and F. Abbate, Chem. Phys. Lett. **264**, 667 (1997).
[24] A. Dogariu, D. Vacar, and A. J. Heeger, Phys. Rev. B **58**, 10 218 (1998).
[25] R. C. Powell and Z. G. Soos, J. Lumin. **11**, 1 (1975).
[26] U. K. A. Klein, R. Frey, M. Hauser, and U. Gösele, Chem. Phys. Lett. **41**, 139 (1976).
[27] J. Gierschner, H.-J. Egelhaaf, and D. Oelkrug, Synth. Met. **84**, 529 (1997).
[28] F. S. Dainton, C. T. Peng, and G. A. Salmon, J. Phys. Chem. **72**, 3801 (1968).
[29] D. Oelkrug, S. Reich, F. Wilkinson, and P. A. Leicester, J. Phys. Chem. **95**, 269 (1991).
[30] N. F. Colaneri, D. D. C. Bradley, R. H. Friend, P. L. Burn, A. B. Holmes, and C. W. Spangler, Phys. Rev. B **42**, 11 670 (1990).
[31] A. R. Brown, K. Pichler, N. C. Greenham, D. D. C. Bradley, R. H. Friend, P. L. Burn, and A. B. Holmes, Synth. Met. **55**, 4117 (1993).
[32] A. Tompert, D. Oelkrug, D. R. Worrall, and F. Wilkinson (unpublished).
[33] R. Österbacka, M. Shkunov, D. Chinn, M. Wohlgenannt, M. Delong, J. Viner, and Z. V. Vardeny, Synth. Met. **101**, 226 (1999).
[34] M. P. T. Christiaans, M. M. Wienk, P. A. van Hal, J. M. Kroon, and R. A. J. Janssen, Synth. Met. **101**, 265 (1999).
[35] B. Kraabel, D. Hulin, C. Aslangul, C. Lapersonne-Meyer, and M. Schott, Chem. Phys. **227**, 83 (1998).
[36] C. Zenz, G. Cerullo, G. Lanzani, W. Graupner, F. Meghdadi, G. Leising, and S. De Silvestri, Phys. Rev. B **59**, 14 336 (1999).
[37] M. Liess, Z. V. Vardeny, and P. A. Lane, Phys. Rev. B **59**, 11 053 (1999).